SCALING OF CAVITATION EROSION PROGRESSION WITH CAVITATION INTENSITY AND CAVITATION SOURCE

Jin-Keun Choi, Arvind Jayaprakash, and Georges L. Chahine
DYNAFLOW, INC.
10621-J Iron Bridge Road, Jessup, MD 20794 U.S.A.
jkchoi@dynaflow-inc.com

ABSTRACT

A simple mathematical expression is presented to describe cavitation mean depth of erosion versus time for cavitating jets and ultrasonic cavitation. Following normalization with a characteristic time, t^*, which occurs at 75% of the time of maximum rate of erosion, and a corresponding material characteristic mean erosion depth, h^*, the normalized erosion depth is related to the normalized time by $\bar{h} = 1 - e^{-\bar{t}^2} + e^{-1}\bar{t}^{1.2}$. This was obtained by conducting systematic erosion progression tests on several materials and varying erosion field intensities. Both a modified ASTM-G32 method and DYNAFLOW's cavitating jets techniques were used and the jet pressures were varied between 1,000 and 7,000 psi. The characteristic parameters were obtained for the different configurations and the correlation was found to be very good, exceeding an R^2 of 0.988 for all cases. Relationships between these parameters and the jet pressure were obtained and resemble familiar trends presented in the literature for mass loss. The study allowed a comparative evaluation and ranking of the various materials with the two accelerated erosion testing methods used. While several materials ranked the same way with the different erosion intensities and testing method, the relative ranking of erosion resistance of some materials was seen to be dependent on the cavitation intensity.

Keywords: Cavitation erosion; Erosion testing; Steel; Non-ferrous metals; Erosion modeling

1 INTRODUCTION

Prediction of cavitation erosion performance of a new material is a very difficult endeavor as it involves good knowledge of both the material and the cavitation environment to which it will be subjected. This prediction is, however, commonly expected or required as one designs a new turbo machinery blade or propeller or addresses whether a new claimed 'advanced' material will provide the promised performance. To do so, the industries have to rely on laboratory testing, using accelerated erosion testing methods and comparative tests between the new material and previously used materials. This raises questions, such as: a) How to transpose the accelerated test results to the operation at full scale of the new design? b) How accurate is it to accept that ranking and quantitative erosion rate ratios remain the same between the accelerated method erosion tests and the full scale erosion, especially that previous studies indicate that the erosion resistance of materials sometimes depends on the intensity of the cavitation field [1-6]. There have been numerous recent studies to better understand the cavitation erosion and attempts to model the physical process involved [7-14].

With the continual desire to increase ship speeds and carrying capacity motivated by increased economic benefits of higher speed transportation or larger payload, the hydrodynamic loading on propellers has significantly increased over the past decades [15]. As a result, potential for cavitation erosion on various parts of the ship control and propulsion system, such as propeller blades, hub,

rudders, nearby ship stern sections, etc. continues to increase along with the search for better erosion resistant materials.

Proper evaluation of new materials for their resistance to cavitation erosion requires a comprehensive effort contrasting the "*intensity*" of the cavitation field with the "*resistance*" of the material. In absence of historical data on the performance of a proposed new material in the target cavitating flow fields, the designer and the decision maker have to rely on laboratory experimental studies. Field erosion studies have been conducted for hydraulic turbines and pumps (e.g. [15-19]), but for marine applications small scale laboratory tests are more common. The laboratory experimental studies aim at determining within required short time periods an evaluation of the new material, whereas in the real field cavitation erosion is expected to not occur but after a long duration of exposure. Such accelerated erosion test techniques include the utilization of ultrasonic vibration to generate the cavitation [20-22], cavitation flow loops with strong flow separation or venturi effects [23-26], and submerged cavitating jets [6,27-29] among other methods. There are also attempts to test the model propeller in the water tunnel [30]. Some of these techniques are standardized and follow the American Society for Testing and Materials (ASTM) Standards [31]. The ultrasonic technique and the liquid jet technique are the two most popular laboratory techniques for testing cavitation erosion characteristics of materials. In the present study, the ultrasonic cavitation and cavitating jets at different intensity were used.

In this paper, we follow the progression of erosion (i.e., time history of material loss) and represent the progression using a mathematical function. This is comparable to previous attempts to use Weibull functions to describe the mass loss curves [32]. This was not used here as is, since Weibull functions have the limitation that the terminal erosion rate (as time goes to infinity) has to be zero. In this paper, we propose an improved mathematical model to erosion progress, and show that it is useful to compare different erosion progressions for different materials under a large range of cavitation intensities for both cavitating jet and ultrasonic cavitation.

The aim of the current work is to understand the relative aggressivity of the cavitation fields generated by ultrasonic cavitation and jet cavitation of various driving pressures and to identify the relative erosion resistance ranking of the tested materials. The dependency of such ranking on the cavitation intensity is also addressed in this study.

2 BACKGROUND: MATERIALS RESPONSE TO CAVITATION LOADS

Cavitation erosion, no matter where and how it is generated, results from the repeated impulsive loading of the material by high intensity short duration pressures loads, due to shock waves and bubble reentrant jet impacts [23,24,34-37]. These are difficult to measure but can be inferred from acoustic signals and pit measurements [7,27,29,33]. Statistical correlations can be obtained between these measurements and can be associated with the facility producing the erosion and with empirically accepted cavitation intensity indicators, such as flow speed, ambient pressure, amplitude and frequency of ultrasonic horn, etc. While "weak" materials may fail rapidly under the repeated shock waves and jet impacts, a more "resistant" material will accumulate stain and experience over a long period the symptoms of fatigue. Initially the material surface gets deformed and is modified microscopically without any loss of material (*incubation period*). This is accompanied by work hardening of the surface. Cavitation peening techniques take advantage of this phase to render the material more resistant to stress. During this initial phase, permanent deformation may occur, sometimes accompanied with plastic flow and local displacement of material micro particles, as well as the development in the later stage of micro-cracks for brittle materials. On a weight loss versus time curve (Figure 1) this is the initial very short period where little material loss is observed. This can be difficult to observe in some accelerated tests, but its duration is actually very important to the determination of the life extent of the cavitating device (e.g. propeller in the full scale application).

Following this period, the erosion process accelerates.

It is known that the weight loss curve has an S shape, as illustrated in Figure 2, which shows an erosion acceleration phase during which the erosion rate increases until attaining a maximum. This is called the *Accumulation* or *Acceleration Period*. In this phase, the material experiences increased fracture and weight loss following the end of hardening in the incubation period. The extent of this zone depends upon the strain-hardening properties of the material and involves microscopic chunks of material being removed following propagation of large cracks in between the grains of the material. The accumulation period ends once the surface properties of the material have changed so much that an interaction begins to occur between the new material surface shape and the cavitation region. The new roughness affects the cavity dynamics and entrapped gas and liquid in the deep craters start cushioning the bubble collapse. This time period is known as the *Attenuation Period* (or *Deceleration Stage*). Finally, a local equilibrium between the erosive power of the cavitation field and the response of the material occurs and the erosion process enters the *Steady-State Period* (or *Terminal Stage*), where the rate of weight loss reaches a quasi constant value, or a linear behavior of the weight loss S-Curve. The clear separation between the four regions described above depends on the type of materials.

Since the first three stages of the cavitation erosion are quite unsteady and dynamics, correlations between various scales, various materials, or between accelerated and real field tests have concentrated in previous work mostly on the characteristics of the steady-state period [1,2]. Since the erosion rate in that region is constant it has been used to characterize the material. This does not however work for a weak coating which may fail and delaminate before getting to this stage. A new approach we present in this paper is to fit the full time history curve with a single mathematical function.

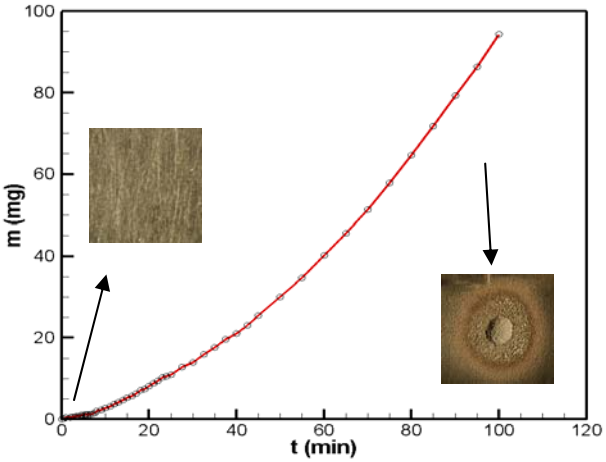

Figure 1. Erosion progression curve for aluminum 1100-0 obtained in a cavitation jet erosion test. Inserts show a picture during the incubation period and another picture during the acceleration period.

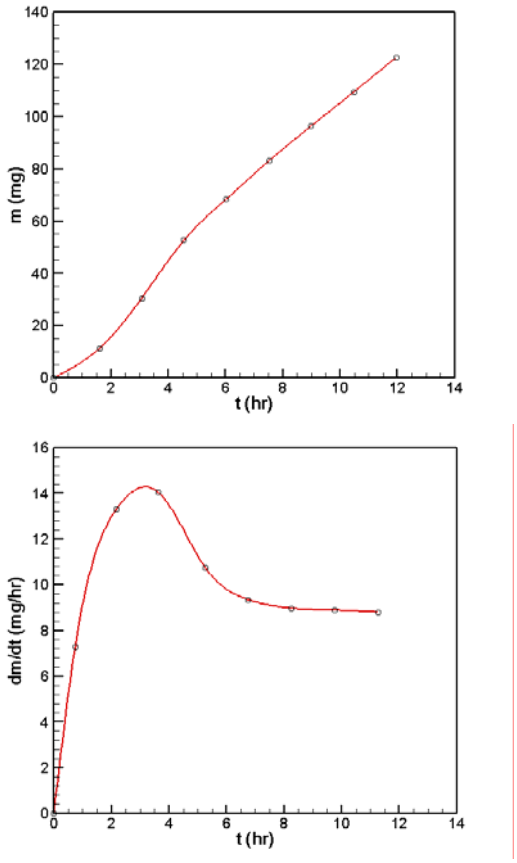

Figure 2. Typical G32 test erosion curves: weight loss S-Curve and erosion rate vs. time curve.

3 ACCELERATED EROSION TESTS

Several laboratory techniques to generate cavitation have been used conventionally to study cavitation erosion in a controlled environment and in an accelerated manner. *Accelerated erosion* tests involve subjecting the considered material to an erosion field that is significantly more "intense" than the actual cavitation that the studied material will be subjected to (so far, using either much higher 'repetition rate' of the cavitation events, more energetic events, more developed cavitation, or a combination of these). However, there are reasons to believe that this choice has to be done much more scientifically than is often practiced, since the objective should be to accelerate the erosion while not subjecting the material to a different cavitation regime or another range of load levels.

Accelerated erosion laboratory techniques include ultrasonic flows, cavitation flow loops with strong flow separation, rotating disks, cavitating venturi flows, vortex generators, and submerged cavitating jets [20-29]. Some of these techniques are standardized by the American Society for Testing and Materials (ASTM) Standards and include Standard G-32 "*Test Method for Cavitation Erosion Using Vibratory Apparatus*" and G-134 "*Test Method for Erosion of Solid Materials by a Cavitating Liquid Jet*" [31]. The ultrasonic technique and the liquid jet technique are the two most popular techniques for testing cavitation erosion characteristics of materials, and the results from both methods will be studied here when eroding the same materials.

3.1.1 Ultrasonic Cavitation Erosion Testing – ASTM G32

In ultrasonic cavitation tests, the cavitation is generated by a vibratory device employing a magnetostrictive ultrasonic horn. A sample "button" of the material being tested is affixed to the end of the horn and is subjected to cavitation resulting from the vibrations of the horn. A cavitation hemispherical cloud forms at the tip of the horn and executes severe dynamics resulting in bubble cloud growth and collapse. In an "alternative" G-32 test configuration (also known as a *stationary specimen method*), the horn tip is placed at a small distance from the stationary material sample and a rather cylindrical cavitation cloud is generated in between the sample and the face of tip of the horn equipped with a strongly cavitation resistant "button" (e.g. Titanium). In the standard G-32 test the temperature, liquid beaker volume, horn tip submergence beneath the free surface, frequency, and amplitude of the oscillations are all prescribed by the ASTM method [31]. Our tests presented in this paper deviated from the ASTM G32 in selecting (for both direct and alternative methods) a sample diameter of 0.5 inch instead of 0.626 inch.

The usual test procedure is to expose the sample to cavitation for a selected period of time, interrupt the test, remove the sample, and record weight to enable calculation of weight loss as a function of time. The sample is then returned for additional time intervals of erosion. In this study, we also recorded other characteristics such as volume of erosion imprint, maximum width and depth, and took photographs of the evolution of the eroded region. Figure 3 shows examples of eroded samples tested by the ultrasonic cavitation.

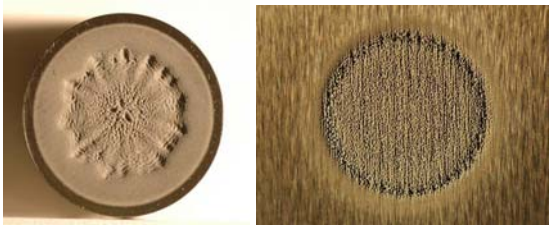

Figure 3. Ultrasonic technique eroded samples pictures. Left: Tested G32 metallic button sample; Right: eroded composite material sample from the alternative G32 method.

3.1.2 Cavitating Jets – ASTM G134 and others

Cavitation intensity produced by cavitating jets can be varied in a very wide range through adjustment of the type of jet, the jet velocity, the jet diameter, the jet angle, the standoff distance, the ambient pressure in which they are discharged [28]. This flexibility makes a cavitating jet a great research and test tool to

study parametrically the effect of cavitation intensity on materials behavior. The cavitation generated by a cavitating jet provides realistic cavitation bubble clouds with distribution of various size micro bubbles, shear flows with vortices, and dense bubble clouds, which collapse on the sample. With the control of the operating pressure, the jet angle, and the stand-off, the testing time can be adjusted to provide either quick erosion for initial screening or time-accelerated erosion more relevant to the real flows.

The cavitating jet erosion test setup used in this study consisted of a DYNAJETS®, cavitating jet nozzle, a sample holder, a water tank, and a pump. The sample holder ensured that the sample was placed back precisely at the same location when it was returned from any examination. The nozzle and the sample were submerged in the water tank so that the sample was subjected to only cavitation bubbles but not to water droplet impacts. A photograph showing a typical setup of the jet nozzle and the sample in its holder is shown in Figure 4. The overall test procedure is similar to that of the G32 tests other than using a cavitating jet. The time intervals are appropriately selected to capture a cumulative weight loss curve displaying as much as possible the characteristic S-curve.

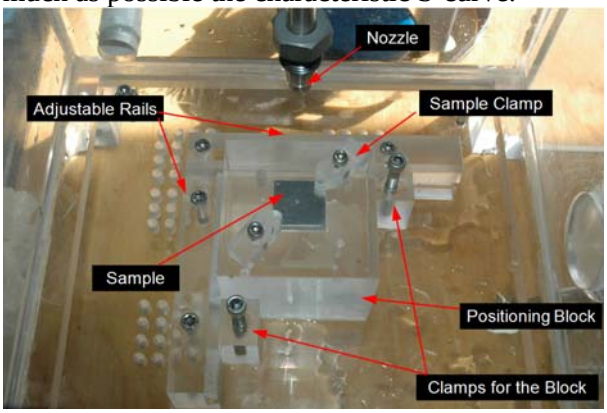

Figure 4. Nozzle and sample holder in the DYNAFLOW's "7 ksi - 5 gpm" cavitation jet erosion test loop.

4 EROSION PROGRESSION FOR DIFFERENT CAVITATION INTENSITIES

In pursuit of definitions of the "*intensity of the cavitation*" in the flow filed and the "*resistance of the material*" to the cavitation erosion, we have conducted systematic tests and obtained erosion data on several materials under various cavitating jet pressures (speeds) and ultrasonic cavitation. Table 1 shows the materials tested, while the various cavitation intensity fields are described further down.

Substrate	Coating
Aluminum 7075	None
Stainless Steel 316	None
Stainless Steel A2205	None
Nickel Aluminum Bronze (NAB)	None
High Yield Stress Steel (HY-80)	None
Aluminum 1100-O	None
Aluminum 7075-T651	Anodized
Low Temperature Colossal Super-Saturation (LTCSS) on Stainless Steel A2205 [38]	LTCSS

Table 1. Materials tested in this study.

4.1 Mathematical Representation of Long Duration Erosion Progression History

In order to study the effect of the imparted cavitation field energy on the evolution of the cavitation erosion over a long period of time, a set of erosion tests were conducted at different jet pressures. The test data were expressed by mathematical erosion curves so that the jet pressure effect can be sought for the whole erosion history of different cases. To account for differences in densities of different materials and the size of the cavitation area, the erosion time history is presented in terms of *mean depth of erosion* (MDE), h, versus time, defined as:

$$h(t) = \frac{m(t)}{\rho A(t)}, \qquad (1)$$

where $m(t)$ and $A(t)$ are the mass loss and eroded area at time t, and ρ is the material density.

Figure 5 shows an example of the mean depth of erosion of Al 7075-T651 subjected to the G32 ultrasonic cavitation field and to a set of cavitating jets with different pressures across the nozzle. The erosion curve marked with G73 is obtained from a liquid impingement erosion test on the same material following the ASTM G73 standard [31]. The figure illustrates that both the jets and the ultrasonic device result in similar shape MDE curves with the G32 falling a little below the 1,000 psi cavitating jets used in these tests (other tests indicate that G32 is more similar to a 700-800 psi DYNAJETS®). Data points with symbols are from the actual measurements, while the curves are representation of the erosion data using the following mathematical expression:

$$h = 0, \qquad t' = t - t_{inc} \le 0,$$
$$h = h_1\left(1 - e^{-t'^{n}}\right) + h_2 t'^{\beta}, \tag{2}$$

where t_{inc} is the incubation time, h_1, h_2 are depth constants and n and β are time parameters which characterize the cavitation erosion progression.

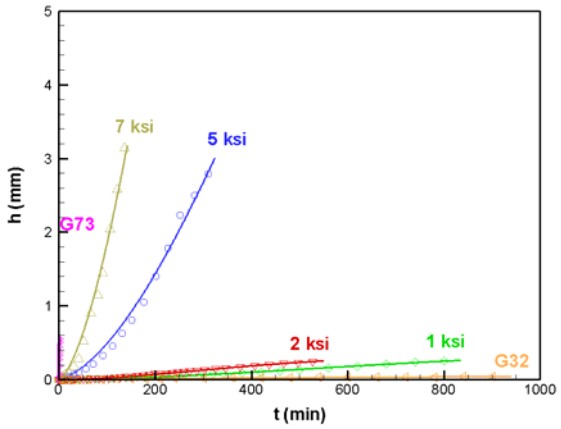

Figure 5. Cavitation erosion average depth versus time on AL7075 resulting from a DYNAJETS® nozzle cavitation at different nozzle pressures (jet velocities). The solid lines are analytical curves obtained from the mathematical erosion evolution model shown in Equation (6).

4.1.1 Definition of the Characteristic Scales

Equation (2) can be normalized using a characteristic depth, h^*, and a characteristic time, t^*, and defining $\bar{h}$ as the normalized erosion depth by and $\bar{t}$ as the normalized time :

$$\bar{h} = \frac{h}{h^*}, \quad \bar{t} = \frac{t - t_{inc}}{t^*}, . \tag{3}$$

This leads to the following MDE normalized equation:

$$\bar{h} = 1 - e^{-\bar{t}^{n}} + \alpha \bar{t}^{\beta}. \tag{4}$$

The constants, n, α, and β, are parameters which characterize the cavitation erosion progression and were found in our tests to date, illustrated by the examples in Figure 5, as having the values:

$$n = 2, \quad \alpha = 1/e = 0.37, \text{ and } \beta = 1.2. \tag{5}$$

The erosion evolution was therefore found to be characterized by:

$$\bar{h} = 1 - e^{-\bar{t}^2} + \frac{1}{e}\bar{t}^{1.2}. \tag{6}$$

All three parameters (h^*, t^*, and t_{inc}) are characteristics of the response of the specific material to the particular cavitation erosion field. For all times less than t_{inc} there is no weight loss of the material. h^* and t^* are such that $h = h^*$ at $t - t_{inc} = t^*$, or $\bar{h} = 1$ at $\bar{t} = 1$. The first and the second derivatives of the normalized MDE can be derived for this case:

$$\frac{d\bar{h}}{d\bar{t}} = 2\bar{t}\, e^{-\bar{t}^2} + \frac{1.2}{e}\bar{t}^{0.2}, \tag{7}$$

$$\frac{d^2\bar{h}}{d\bar{t}^2} = 2e^{-\bar{t}^2}\left(1 - 2\bar{t}^2\right) + \frac{0.24}{e}\bar{t}^{-0.8}. \tag{8}$$

These two functions are shown in Figure 6, which illustrates that the mean erosion depth rate achieves its maximum when $t = 0.75t^*$. This provides a good interpretation for t^*, as being 4/3 the time at which the rate of the mean depth of erosion attains its maximum. It would have been more eloquent to change variables to have the maximum at t^*, but this would affect the simplicity of Equation (6), which is very easy to remember in the present form.

Figure 7 shows all Figure 5 data in a normalized format and illustrates the good quality of the matching of the mathematical model, Equation (6), to the experimental data. Notice that specific tests cover different ranges of the erosion curve, but all test data fall on one standardized shape of erosion curve. Figure 8 shows the corresponding normalized erosion rate ($d\bar{h}/d\bar{t}$) curves, which fall on one curve as expected. Table 2 shows the standard deviation of the error when the measured data are expressed by Equation (6). The normalized standard deviation is small and is seen to be of the order of 1 ~ 3% in all cases. The coefficient of determination ($R^2 = 1 - \left[\sum (y_i - f_i)^2 / \sum (y_i - \bar{y})^2\right]$) represents how well the prediction (f_i) describes the actual data (y_i). The same data and curves are shown in log-log scale in Figure 9 in order to enhance the various regions of the history. It is noticeable that the empirical representation curve fits are good from the acceleration stage to the terminal erosion stage, but obviously do not capture the incubation period where the erosion depth is almost zero.

The characteristic erosion depth, h^*, and the characteristic time, t^*, are directly related for a given material to the cavitating jet speed (or upstream pressure). This is illustrated in Figure 10. As expected, the characteristic erosion depth increases and the characteristic erosion time decreases as the cavitation intensity (i.e. the jet pressure) increases. The scaling relationship from this data set can be expressed as:

$$h^* = 8\times10^{-5}\left(\Delta p_{jet}\right)^{2.2163},\ h^* \text{ in } \mu\text{m},\ \Delta p_{jet} \text{in psi}, \quad (9)$$

$$t^* = 132.7\left(\Delta p_{jet}\right)^{-0.3547},\ t^* \text{ in hour},\ \Delta p_{jet} \text{in psi}. \quad (10)$$

Using the relationship between the jet pressure and the jet velocity, the above scaling relationship can be expressed using the jet velocity as follows:

$$h^* = 2.4\times10^{-7}\left(V_{jet}\right)^{4.4326},\ h^* \text{ in } \mu\text{m},\ V_{jet} \text{ in m/s}, \quad (11)$$

$$t^* = 337\left(V_{jet}\right)^{-0.7094},\ t^* \text{ in hour},\ V_{jet} \text{ in m/s}. \quad (12)$$

The exponent 4.43 over the jet velocity in the erosion depth expression is consistent with the typical values of 4 ~ 5 reported in literature [1,2].

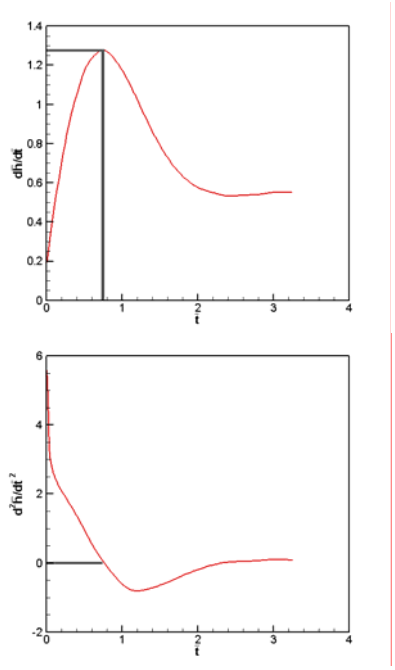

Figure 6. Cavitation erosion mean depth of erosion rate, $d\bar{h}/d\bar{t}$, (top) and its time derivative, $d^2\bar{h}/d\bar{t}^2$, (bottom) versus nondimensional time, $\bar{t}$, as described by the mathematical erosion evolution model shown in Equations (6) to (8). Maximum erosion depth rate, $\left(d\bar{h}/d\bar{t}\right)_{\max}$, occurs when $t = 0.75t^*$.

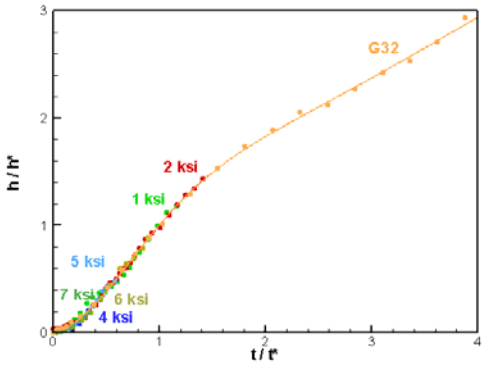

Figure 7. Normalized cavitation erosion average depth versus normalized time on AL7075 resulting from DYNAJETS cavitation at different nozzle pressures (jet velocities) and G32. The solid line is obtained from the mathematical erosion progression model shown in Equation (6).

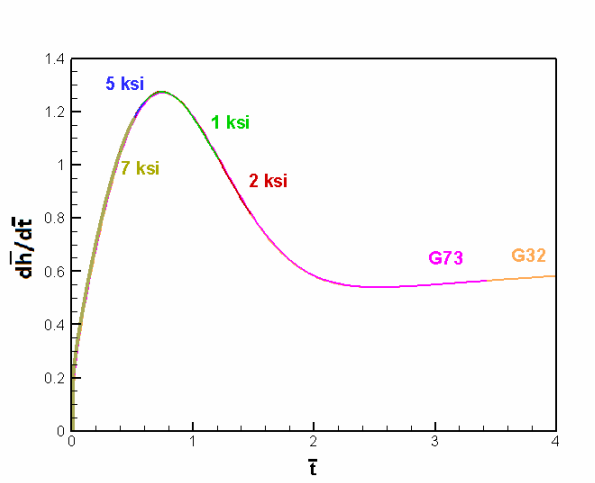

Figure 8. Comparison of normalized erosion rate curves of AL7075 erosion data obtained by various test methods.

Test Method and Intensity	h*, mm	t*, min	h*/t*, mm/min	Standard Deviation in *h/h**	Coefficient of Determination, R^2
G32	0.041	232	1.8 e-4	2.4%	0.9985
1,000 psi Jet	0.593	689	8.6 e-4	3.2%	0.9920
2,000 psi Jet	0.482	373	1.3 e-3	2.2%	0.9972
5,000 psi Jet	16.3	533	3.1 e-2	1.4%	0.9919
7,000 psi Jet	22.0	274	8.0 e-2	1.4%	0.9882

Table 2. Normalized standard deviation or error in expressing the erosion data with Equation (6).

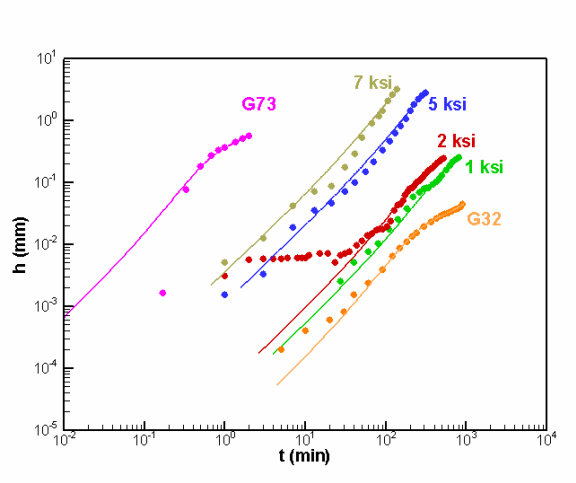

Figure 9. Cavitation erosion average depth versus time on AL7075 resulting from a DYNAJETS nozzle cavitation at different nozzle pressures (jet velocities) shown in log-log scales. The solid lines are analytical curves from the mathematical erosion model shown in Equation (6). The almost horizontal initial 2 ksi dots correspond to the incubation period.

4.2 G32 and Cavitating Jet Erosion for Different Materials

This section considers a set of erosion tests on different materials and examines whether the proposed mathematical model applies to these different materials. An example of G32 raw test data - erosion depth versus time - for various materials is shown in Figure 11. The corresponding curves using the mathematical expressions from Equation (6) with the best fits are also shown. Figure 12 shows the model curve with all the normalized data fallen on it. This graph shows the mass loss normalized by the characteristic mass, *m** which corresponds to the characteristic MDE, *h**. It is noticeable that the individual erosion curves cover different portions of a common S-shaped normalized curve depending on the erosion resistance and the test duration. As we can see, the erosion progression data for all materials is very well fitted with the mathematical expression (6).

Similarly, DYNAJETS® cavitating jets erosion tests were conducted with a 5,000 psi jet for the same materials presented in Figure 11 for

G32. The cavitating jet results are shown in Figure 13. Here again, all of the data are also relatively very well fitted with the mathematical expression (6). Figure 14 shows the normalized erosion time history of the three selected materials (aluminum, nickel aluminum bronze, and stainless steel) under various erosion intensities. A nice collapse onto one normalized S-curve is well demonstrated.

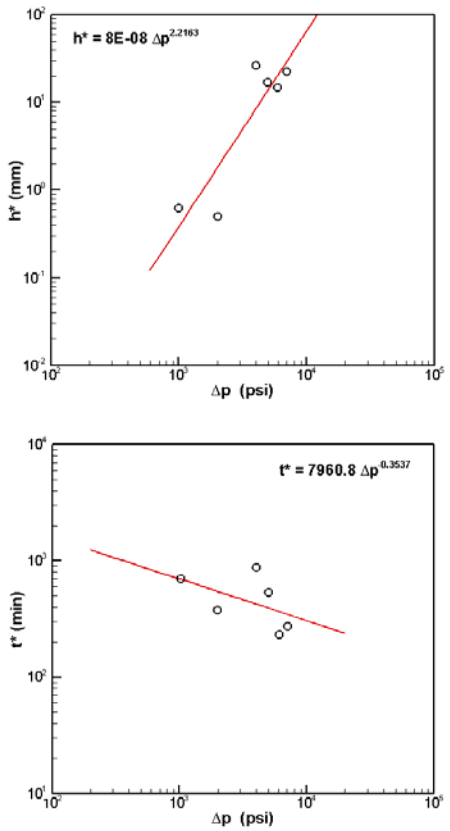

Figure 10. Scaling of the characteristic erosion depth, h*, (top) and the characteristic time, t*, (bottom) with the cavitating jet nozzle pressure.

4.3 Discussion

A mathematical description of the erosion time history, as presented above, is very useful in the task of comparing cavitation erosion behavior of different materials exposed to the same or different known cavitation intensity, and where individual erosion tests were conducted under different cavitation intensities or different duration of erosion exposure. It appears that the overall cavitation erosion resistance to a cavitation field is characterized by the two parameters: *h**, the characteristic mean erosion depth and *t**, the characteristic erosion time, with the *characteristic erosion rate* defined as *h*/t**.

Table 3 and Table 4 show the numerical coefficients used to fit the erosion data of the different materials tested by the G32 method and the 5,000 psi jet cavitation. In these tables, the materials are listed in the order of increasing characteristic erosion rate. The rankings by the two test methods in Table 3 and Table 4 agree in general, but a couple of materials did not rank the same way. For example, HY80 was more resistant than SS 316 in G32 tests, but the order reversed in the 5,000 psi cavitating jet tests. From the observed erosion rates of the two test methods, it is obvious that the cavitation field of a 5,000 psi jet is much more intense and erosive than the cavitation field generated in G32 ultrasonic tests. This tells that, relative to SS 316, HY80 has greater resistance in a weaker cavitation field but is less resistant in an intense cavitation field. Comparing NAB and LTCSS is also interesting. The LTCSS shows higher erosion resistance than NAB in the weaker cavitation field of the G32 test, but not in the intense cavitation field of 5,000 psi jet cavitation test. These tell that the material erosion response of some materials depends on the intensity of the cavitation field.

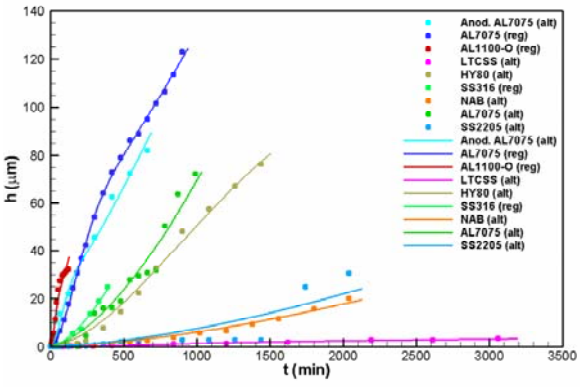

Figure 11. Mean depth of erosion (based on mass loss) vs. time curves obtained from G32 tests for various materials. Solid lines are fits of the data with the mathematical model of Equation (6). Modified ASTM G32 method was used in these tests; (reg) represents the direct method, (alt) represents the alternative method.

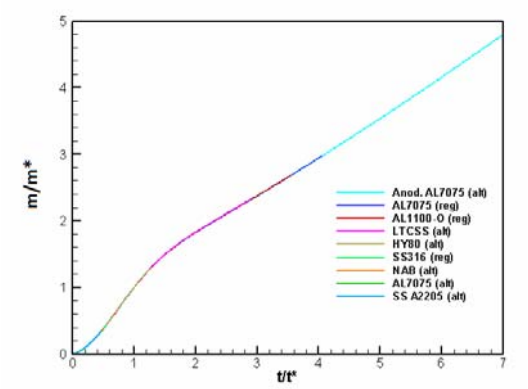

Figure 12. Curves of the normalized mass loss vs. normalized time. m* is the characteristic mass loss. All curves start from the origin, but for the same physical time, the tested materials reached different erosion stages.

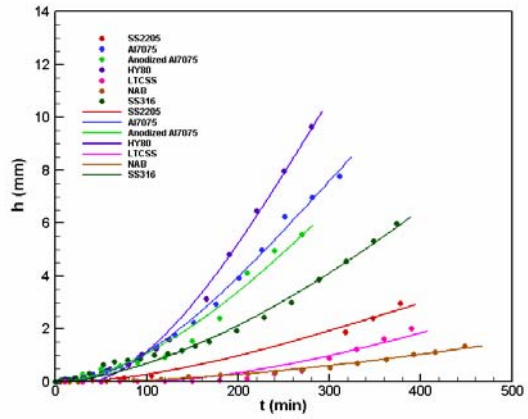

Figure 13. Mean depth of erosion (based on mass loss) vs. time curves obtained from a 5,000 psi jet cavitation and curve fits of the data to the mathematical model shown in Equation(6).

Table 5 shows a comparison of the erosion rates of the materials as obtained by the two accelerated erosion methods using different levels of cavitation intensity. The ratios of the erosion rates between the jet at 5,000 psi and the G32 method, for example, vary vastly from material to material. This ratio varies by two orders of magnitudes between the weakest and the strongest erosion resistant materials and is, as expected, very high for the strongest materials as for these the high intensity jets produce significant erosion, while the G32 is just at the limit of solicitation of the material.

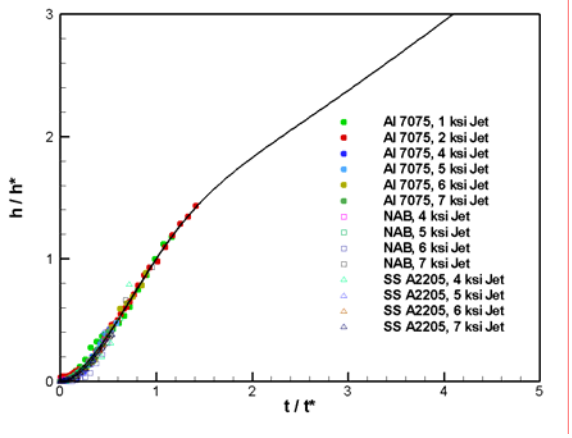

Figure 14. Curves of the normalized erosion depth vs. normalized time for Aluminum, NAB, and stainless steel tested with cavitating jets at various pressures. Curves are the mathematical expressions (6) and the symbols are the measured data points.

Material Tested with G32 Alternative Method	Characteristic Erosion Depth, h* , mm	Characteristic Time, t* , min	Characteristic Erosion Depth Rate, h*/t*, μm/min
LTCSS	0.0014	1100	0. 001
NAB	0.0498	4190	0. 012
SS A2205	0.0693	4520	0. 015
HY80	0.0622	1180	0. 053
SS316	0.0621	771	0. 081
AL7075	0.197	2100	0. 094
AL7075	0.0419	232	0. 181
Anodized AL7075	0.0186	98	0. 190
AL1100	0.0139	35	0. 392

Table 3. Parameters of the erosion mathematical model and characteristic erosion rates for the different material tested with G32 ultrasonic tests. The materials are ordered by increasing value of the characteristic erosion depth rate.

Material Tested with 5,000 psi Cavitating Jet	Characteristic Erosion Depth, h^* , mm	Characteristic Time, t^* , min	Characteristic Erosion Depth Rate, h^*/t^*, μm/min
NAB	4.3	941	4.57
LTCSS	4.0	348	11.5
SS A2205	14.2	776	18.3
SS316	17.9	804	22.2
Anodized AL7075	15.0	533	28.3
AL7075	11.0	374	29.5
HY80	9.7	223	43.8

Table 4. Parameters of the erosion mathematical model and characteristic erosion rates for the different material tested with 5,000 psi DYNAJETS® cavitating jet tests. The materials are ordered by increasing value of the characteristic erosion depth rate.

A better comparison is to run the two methods – cavitating jets, ultrasonic cavitation – at comparable cavitation intensity. This would be when the jet intensity is in the range of 700~800 psi. The last two columns in Table 5 show such a comparison using the pressure correlations in Figure 10, to deduce the jet erosion rates as these were not obtained experimentally. The erosion rates corresponding to the 750 psi jet were estimated from the 5,000 psi jet results using the exponents 2.22 and –0.35 in (9) and (10). These estimated erosion rates are comparable to those obtained from G32 tests, as the ratios in the last column are mostly of order 1. This indicates that the exponents on the jet pressure in (9) and (10) obtained from tests using Al 7075 may be applied to other materials, and that the cavitation intensity of G32 tests is similar to that of the 750 psi cavitating jet. One exception is noticed for LTCSS, which showed extremely low erosion rate from the G32 test. A possible explanation is that the cavitation aggressiveness of G32 is very low for this especially hardened surface of the stainless steel and that it is able to barely exceed the incubation period, while the 5,000 psi jet cavitation proceeds well beyond into the erosion of the material penetrating the hard surface layer after which the erosion proceed in the unhardened steel.

Material	G32 Ultrasonic Alternative, (μm/min)	5,000 psi Cavitating Jet, (μm /min)	Ratio of Erosion rates, 5 ksi Jet / G32)	750 psi Jet, Deduced from 5000 psi results (μm /min)	Ratio of Erosion rates, (750 psi Jet / G32)
NAB	0.012	4.6	381	0.0351	1.2
LTCSS	0.001	11.5	11500	0.0878	38.5
SS A2205	0.015	18.3	1220	0.140	4.1
AL7075 Anodized	0.190	28.3	149	0.216	0.5
AL 7075	0.094	29.5	314	0.225	1.1
HY80	0.053	43.8	826	0.334	2.8

Table 5. Comparison of erosion rates between G32 tests and 5,000 psi cavitating jet erosion tests. Materials are presented ranked by the jet erosion results.

5 CONCLUSIONS

In pursuit of practical definitions of the "*intensity of the cavitation*" of a given cavitating flow field and of the "*resistance of the material*" to cavitation erosion, we have conducted systematic long term erosion tests (i.e. much beyond the incubation period) on several materials using two different accelerated erosion testing methods. The test methods used were the modified ASTM G32 Ultrasonic Cavitation Erosion tests and the DYNAJETS® cavitating jets run at various jet speed or nozzle pressures. Through accelerated erosion testing and analysis a comparative evaluation and energy ranking of the materials and the erosion testing methods were established.

This was done by expressing the erosion progression using a simple mathematical equation with characteristic parameters. A

characteristic time, t^*, which occurs at 75% of the time of maximum rate of erosion, and a corresponding material characteristic mean erosion depth, h^*, were defined. Using these to normalize the mean depth erosion and time, the simple erosion depth time evolution expression found is: $\bar{h} = 1 - e^{-\bar{t}^2} + e^{-1}\bar{t}^{1.2}$. This equation was able to represent all our experimental erosion data for the various cavitation sources and the various materials within only 2~3% deviation (Coefficient of Determination, R^2>0.988). Such a mathematical representation of the erosion time evolution enables one to compare various materials tested under cavitation fields of different intensities following determination of the two characteristic parameters: characteristic mean depth of erosion and characteristic erosion time. The various tested materials were ranked based on their cavitation resistance. Comparisons of the erosion rates from the two accelerated erosion methods using very different levels of cavitation intensity showed that the erosion response of some materials depends on the cavitation intensity. Several other approaches to quantify and understand the dynamics of cavitation intensities are presented in companion publications. These included pitting tests during the incubation period [33] and cavitation field pressure measurements [39]. All these efforts will be eventually combined to provide a practical tool for erosion predictions.

6 ACKNOWLEDGEMENTS

Support for this work was provided by Office of Naval Research (ONR) under contract number N00014-08-C-0450, monitored by Dr. Ki-Han Kim. We are thankful for his support, suggestions, and discussions. The authors would also like to acknowledge Dr. Martin Donnelly, NSWC Carderock Division, Dr. Jean-Pierre Franc, LEGI, Grenoble, France, Dr. Ayat Karimi, EPFL, Lausanne, Switzerland, and Dr. Farrell Martin, NRL, for useful discussion. Finally, the authors would also like to recognize the long hours of efforts by Emmanuel Coleman and Patrick Aley of DYNAFLOW, INC. in conducting the laborious erosion experiments.

REFERENCES

1. A. Thiruvengadam, Handbook of Cavitation Erosion, Hydronautics Technical Report 7301-1, 1974.
2. P. Eisenberg, H.S. Preiser, A. Thiruvengadam, "On the Mechanisms of Cavitation Damage and Methods of Protection," *Trans. Soc. Naval Architects Marine Eng.* **73** (1965) 241–286.
3. M.A. Dominguez Cortazar, Le Cavermod, Modèle Physique de l'érosion de Cavitation: Qualification Expérimentale et Numérique, Thèse Universite Joseph Fourier Grenoble I, 1992.
4. J.L. Reboud, Réponse Impulsionnelle d'un Milieu Elastoplastique: Application a L'étude de l'érosion de Cavitation, Thèse, Institut National Polytechnique de Grenoble, 1987.
5. F. Pereira, F. Avellan, Ph. Dupont, Prediction of Cavitation Erosion: An Energy Approach, *Journal of Fluids Engineering* **120** (1998) 719-727.
6. P.A. March, Evaluating the Relative Resistance of Materials to Cavitation Erosion: a Comparison of Cavitating Jet Results and Vibratory Results, *Proc. Cavitation and Multiphase Flow Forum, ASME* (1987) Cincinnati.
7. H. Soyama, A. Lichtarowicz, T. Momma, E.J. Williams, A new calibration method for dynamically loaded transducers and its application to cavitation impact measurement, *J. Fluids Eng*. **120** (1998) 712-718.
8. S. Hattori, M. Takinami, O. Tomoaki, Comparison of Cavitation Erosion Rate with Liquid Impingement Erosion Rate, 7th Int. Symposium on Cavitation, CAV2009 (2009) Ann Arbor, Michigan.
9. S.M. Ahmed, K. Hokkirigawa, Y. Ito, R. Oba, Scanning electron microscopy observation on the incubation period of vibratory cavitation erosion, *Wear* **142** (1991) 303-314.
10. G. Bregliozzi, A. Di Schino, S.I.-U. Ahmed, J.M. Kenny, H. Haefke, Cavitation wear behavior of austenitic stainless steels with

different grain sizes, *Wear* **258** (2005) 503-510.
11. M. Dular, O. Coutier-Delgosha, Numerical modeling of cavitation erosion, *Int. J. Numer. Meth. Fluids* **61** (2009) 1388–1410.
12. H. Soyama, M. Futakawa, K. Homma, Estimation of pitting damage induced by cavitation impacts, *Journal of Nuclear Materials* **343** (1-3) (2005) 116-122.
13. R. Fortes Patella, J. Reboud, A. Archer, Cavitation Damage Measurement by 3D Laser Profilometry, *Wear* **246** (2000) 59-67.
14. J.-P. Franc, Incubation Time and Cavitation Erosion Rate of Work-Hardening Materials, *Journal of Fluids Engineering* **131** (2009) 021303.1-021303.14.
15. M. Billet, The Special Committee on Cavitation Erosion on Propellers and Appendages on High Powered/High Speed Ships, *24th International Towing Tank Conference (ITTC)*, Volume III, UK, 2005.
16. M. Grekula, G. Bark, Experimental Study of Cavitation in a Kaplan Model Turbine, *4th Int. Symposium on Cavitation*, CAV2001 (2001) Pasadena, CA.
17. M. Farhat, P. Bourdon, Extending Repair Intervals of Hydro Turbines by Mitigating Cavitation Erosion, *CEA Electricity '98 Conference & Exposition* (1998) Toronto.
18. M. Farhat, P. Bourdon, P. Lavigne, R. Simoneau, The Hydrodynamic Aggressiveness of Cavitating Flows in Hydro Turbines, ASME Fluids Eng. Div. Summer Meeting, FEDSM'97 (1997)
19. *Guideline for Prediction and Evaluation of Cavitation Erosion in Pumps*, Turbomachinery Society of Japan, 2010.
20. F.G. Hammitt, C. Chao, C.L. Kling, T.M. Mitchell, D.O. Rogers, Round-Robin Test with Vibratory Cavitation and Liquid Impact Facilities of 6061-T 6511 Aluminum Alloy, 316 Stainless Steel and Commercially Pure Nickel, *Materials Research and Standards*, ASTM, **10** (1970) 16–36.
21. C. Chao, F.G. Hammitt, C.L. Kling, ASTM Round-Robin Test with Vibratory Cavitation and Liquid Impact Facilities of 6061-T6 Aluminum Alloy, 316 Stainless Steel, Commercially Pure Nickel, The University of Michigan Report MMPP-344-3-T / 01357-4-T, **84**, 1968.
22. K.H. Light, Development of a Cavitation Erosion Resistant Advanced Material System, M.S. Thesis, Mechanical Eng., University of Maine, 2005.
23. M.A. Dominguez-Cortazar, J.P. Franc, J.M. Michel, The Erosive Axial Collapse of a Cavitating Vortex: An Experimental Study, *Journal of Fluids Engineering* **119** (1997) 686-691.
24. F.G. Hammitt, Damage to solids caused by cavitation, *Philosophical Trans. of the Royal Society of London*. Series A, Mathematical and Physical Sciences, **260**, 1110, (1966) 245-255.
25. X. Escaler, F. Avellan, E. Egusquiza, Cavitation Erosion Prediction from Inferred Forces Using Material Resistance Data, *4th Int. Symposium on Cavitation*, CAV2001 (2001) Pasadena, CA.
26. J.S. Baker, Cavitation Resistant Properties of Coating Systems Tested on a Venturi Cavitation Testing Machine, Bureau of Reclamation, Research Laboratory and Services Division, Denver, CO, 1994.
27. T. Momma, A. Lichtarowicz, A study of pressures and erosion produced by collapsing cavitation, *Wear* **186-187**, Part 2, (1995) 425-436.
28. G.L. Chahine, P. Courbière, Noise and Erosion of Self-Resonating Cavitating Jets, *Journal of Fluids Engineering* **109** (1987) 429-435.
29. M.K. Lee, W.W. Kim, C.K. Rhee, W.J. Lee, Liquid Impact Erosion Mechanism and Theoretical Impact Stress Analysis in TiN-Coated Stream Turbine Blade Materials, *Metallurgical and Materials Transactions A*, **30A**, (1999) 961-968.
30. W. Pfitsch, S. Gowing, D. Fry, M. Donnelly, S. Jessup, Development of Measurement Techniques for Studying Propeller Erosion Damage in Severe Wake Fields, Proc. 7th Int. Symposium on Cavitation, CAV2009 (2009) Ann Arbor, Michigan.
31. *Annual Book of ASTM Standards – Section 3 Material Test Methods and Analytical Procedures*, American Society for Testing and Materials (ASTM), **03.02**, 2010.
32. Y. Meged, Modeling of the initial stage in vibratory cavitation erosion tests by use of a

Weibull distribution, *Wear* **253**, pp.914–923, 2002.
33. J-P. Franc, M. Riondet, A. Karimi, G.L. Chahine, Material and velocity effects on cavitation erosion pitting, *Wear* **274-275**, pp.248-259, 2012.
34. K.A. Morch, Dynamics of Cavitation Bubbles and Cavitating Liquids, *Treatise on Materials Science and Technology* **16** (1979) 309-355.
35. J.R. Blake, B.B. Taib, G. Doherty, Transient Cavities near Boundaries. Part I. Rigid Boundary, *Journal of Fluid Mechanics* **170** (1986) 479-497.
36. H. Zhang, J. Duncan, G.L. Chahine, The Final Stage of the Collapse of a Cavitation Bubble near a Rigid Wall, *Journal of Fluid Mechanics* **257** (1993) 147-181.
37. G.L. Chahine, T.O. Perdue, Simulation of the Three-Dimensional Behavior of an Unsteady large Bubble near a Structure, *Drops and Bubbles*, Third International Colloquium, Monterey, CA, ed. Taylor G. Wang, American Institute of Physics (1988) 188-199.
38. S. Collins, P. Williams, Low-Temperature Colossal Supersaturation, *Advanced Materials and Processes*, Sep. (2006) 32-33.
39. J-P. Franc, M. Riondet, A. Karimi, G.L. Chahine, Impact load measurements in an erosion cavitation flow, *J. Fluid Eng*. **133**, Dec. 2011.